Nanoscale

ROYAL SOCIETY OF CHEMISTRY

MINIREVIEW

View Article Online
View Journal | View Issue

Cite this: *Nanoscale*, 2021, **13**, 19341

Encapsulation of lead halide perovskite nanocrystals (NCs) at the single-particle level: strategies and properties

Qixuan Zhong, Muhan Cao * and Qiao Zhang *

Received 20th August 2021,
Accepted 28th October 2021

DOI: 10.1039/d1nr05478c

rsc.li/nanoscale

Lead halide perovskite NCs ($APbX_3$, A = formamidinium (FA), methylammonium (MA) or Cs; X = Cl, Br, I or their mixture) have attracted unprecedented attention due to their excellent photophysical properties and wide application prospects. However, the inherent ionic structure of $APbX_3$ NCs makes them very sensitive to external conditions such as water and oxygen, resulting in poor stability. As a feasible strategy, encapsulation is considered to be effective in improving the stability. In this minireview, we focus on single-particle-level coating, which not only can improve the stability but also maintain the nano effect of the original NCs. This review summarizes the fundamental information on $APbX_3$ NCs and the necessity of single-particle-level coating. Subsequently, a variety of heterostructures at the single-particle level are introduced in detail. Then, their applications are summarized. Moreover, we discuss the challenges and prospects of the single-particle-level heterostructures based on $APbX_3$ NCs.

1. Introduction

Metal halide perovskites were first discovered in 1893,[1] but it was not until 2009 that they became a focus of attention, owing to their very first application in photovoltaic devices.[2] In 2015, Kovalenko's group[3] reported, for the first time, the preparation of all-inorganic lead halide perovskite $CsPbX_3$ NCs (X = Cl, Br, I or their mixture). Their excellent photophysical properties, including high brightness, tunable emission, high color purity (narrow emission peak), high light absorption coefficient, and high defect tolerance, make them promising in optoelectronic fields such as solar cells,[4] light-emitting diodes (LEDs),[5,6] and so on. For example, $CsPbX_3$-based LEDs have achieved a high external quantum efficiency (EQE) of 12.3% for blue LED,[5] 22% for green LED,[5] and 23% for red LED.[7] Considering their outstanding properties and promising performance in devices, $APbX_3$ NCs have been regarded as one of the next-generation optoelectronics candidates.[8–11]

For practical applications, stability is a particularly important parameter. $APbX_3$ NCs are suitable for optoelectronic devices; however, their poor stability is a shortcoming that

Institute of Functional Nano & Soft Materials (FUNSOM), Jiangsu Key Laboratory for Carbon-Based Functional Materials & Devices, Soochow University, No. 199 Ren'ai Road, Suzhou 215123, Jiangsu, People's Republic of China.
E-mail: mhcao@suda.edu.cn, qiaozhang@suda.edu.cn

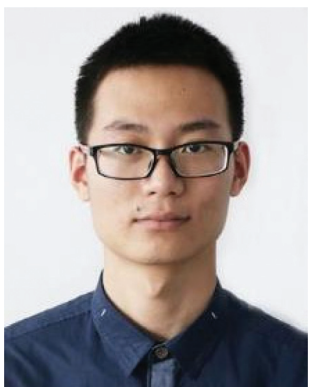

Qixuan Zhong

Qixuan Zhong received his B.S. degree (2016) from Changshu Institute of Technology. He is now a graduate student in the Institute of Functional Nano & Soft Materials (FUNSOM), Soochow University. His current research interests focus on the synthesis and applications of all-inorganic metal halide perovskite/oxide composite materials.

Muhan Cao

Muhan Cao obtained her Ph. D. degree in Environmental Science and Technology from Hohai University in 2015. Now she is an associate research fellow at Soochow University. Her current research interests focus on the design of metal and semiconductor nanocrystals and their applications in optoelectronic fields.

limits their practical applications. The suboptimal stability of $APbX_3$ NCs is mainly attributed to their inherent ionic properties as well as the capping ligands that are dynamically balanced on the surface.[12,13] To enhance durability, a direct and effective method is to prepare highly stable $APbX_3$ NCs encapsulated in an inert shell, such as polymers and oxides.[14,15] These shells can significantly improve the stability of $APbX_3$ NCs against environmental stimuli. Depending on the number of $APbX_3$ NCs in one shell, the encapsulation strategies can be divided into multi-particle and single-particle coating. Multi-particle coating has been extensively studied because of the simple synthetic methods. The resulting products usually have a large particle size, which may reach up to several micrometers.[16–22] This large size limits the applications of $APbX_3$ NCs at the nanometer scale. Moreover, multi-particle aggregations are not conducive to study the influence of the shell on the photoelectric properties of $APbX_3$ NCs. In contrast, single-particle-level coated $APbX_3$ NCs, in which one $APbX_3$ NC is wrapped by one shell, exhibit significantly enhanced stability with the protection of the inert shell. The single-particle-scale modification can well maintain the properties of $APbX_3$ at the nanoscale, ideal for application in some special fields, such as biological imaging.[23] More importantly, the optical and photoelectric properties can be tuned, enabled by passivation of the NC surface.

In this review article, we focus on summarizing the preparations, properties, and applications of encapsulated $APbX_3$ NCs at the single-particle level. The first part introduces the design principle for encapsulated $APbX_3$ NCs. In the second part, $APbX_3$-based heterostructures at the single-particle level are summarized. The third part presents the applications of $APbX_3$-based heterostructures. An outlook from our viewpoint is provided to depict the challenges and opportunities with the single-particle encapsulation of $APbX_3$ NCs in the last part.

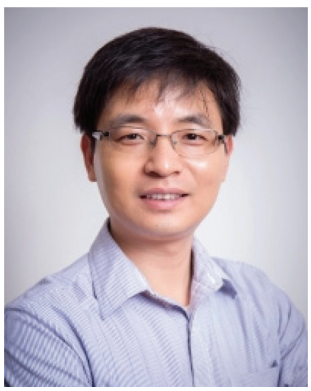

Qiao Zhang

Qiao Zhang is a Professor in the Institute of Functional Nano & Soft Materials (FUNSOM), Soochow University, China. He received his Ph.D. from University of California Riverside (2012). After being a postdoctoral Fellow in the Department of Chemistry, University of California Berkeley (2012–2014), he joined Soochow University in 2014. His main research field is molecular-level studies of surface and heterogeneous catalysis, controllable synthesis of all-inorganic perovskite with tunable optical properties, and their applications.

2. Design principle of encapsulated $APbX_3$ NCs

2.1 Crystal structure of $APbX_3$ NCs

Taking $CsPbX_3$ as an example, Fig. 1a shows a typical cubic $CsPbX_3$ structure, which is highly symmetric. The Pb ion octahedrally coordinates with six halide (X) ions in a $[PbX_6]^{4-}$ configuration, forming a 3D framework perovskite structure through a continuous array of corner-sharing $[PbX_6]^{4-}$ octahedrons. $CsPbX_3$ NCs are ionic compounds that can be easily destructed in the presence of polar solvents. The interactions between $CsPbX_3$ and surface ligands present ionic characteristics as well.[3,38] The dynamic oleic acid (OA) and oleylamine (OLA) are not tightly bound to the surface of $CsPbX_3$ NCs.[39] Instead, proton exchange between coordinated OLA and OA may induce the detachment of ligands (Fig. 1b), resulting in more trap sites and poor optoelectronic performance.[39,40] Fully considering the application occasions of $CsPbX_3$ NCs, environmental stimuli, including light, humidity, heat, and oxygen, will cause the collapse of their structure and quenching of optical properties. Therefore, $CsPbX_3$ NCs with high stability and excellent photoelectric properties are urgently required.

2.2 Single-particle-level coated $APbX_3$ NCs

In recent years, some works have been reported to prepare highly stable core/shell $APbX_3$ NCs. Researchers have developed a variety of strategies for encapsulation of $APbX_3$ NCs with inert materials to enhance their stability against environmental stimuli.[13,41–43] The multi-particle coating strategy has been widely reported because of its mild reaction conditions. Amorphous inert materials, including polymers,[44–46] silica,[22,47] alumina,[20] *etc.*, are usually selected as shell materials to prepare stable structures. Although the coated perovskites exhibit excellent stability, the obtained samples are usually large and even in bulk form, no longer having the superior properties of nanoscale particles that can be used for important applications, *e.g.*, nanoscale optical research and biological fields. Therefore, it is urgently desired but still challenging to synthesize nanosized encapsulated $APbX_3$ NCs that are normally single-particle coated.

Here, we list the difficulties in preparing single-particle coated $APbX_3$ NCs: (1) surface ligand intervention. Most of the

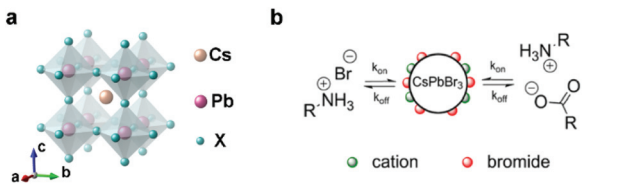

Fig. 1 (a) Schematic of the cubic perovskite lattice. (b) Schematic representation of the dynamic surface stabilization by oleylammonium bromide, oleylammonium oleate and OLA. Reproduced with permission from ref. 39. Copyright 2016 American Chemistry Society.

reported $APbX_3$ NCs are hydrophobic because their surface is covered by long-alkyl-chain ligands. Since some of the reported shell materials, such as SiO_2 and Al_2O_3, are hydrophilic, it is not easy to grow hydrophilic materials onto the hydrophobic surface directly. (2) Restriction of overgrowth conditions. Some shell materials have to be prepared in the presence of high temperature or polar solvents (such as water). However, unprotected perovskite materials cannot withstand such harsh preparation conditions. (3) Lattice mismatching. To realize the coating of crystalline materials, lattice matching needs to be considered. Due to the particularity of the perovskite structure, it will be better to introduce lattice-matched materials as the shell of $APbX_3$ NCs. Many efforts have been made to overcome these problems to prepare single-particle-coated $APbX_3$ NCs. In the next section, we will summarize some typical cases according to different shell materials.

3. $APbX_3$-based heterostructures

Depending on shell materials, this section is divided into four parts: $APbX_3$/oxide, $APbX_3$/semiconductor, $APbX_3$/metal, and others. The growth mechanism and photophysical properties of different core/shell heterostructures are discussed in this section, and a comparation of the stability before and after encapsulation is listed in Table 1.

3.1 $APbX_3$/oxide

Inert oxides with high stability, such as SiO_2 and Al_2O_3, are regarded as alternative shell materials for protecting $CsPbX_3$ NCs due to their weak light absorption and simple preparation strategies.[48] Most of the reported structures are multi-particle coatings, probably due to the uncontrollable reaction conditions and the destruction of $APbX_3$ NCs by polar byproducts. Precisely controlling the growth of oxides on the core is particularly important for achieving single-particle-level coating by oxides. This section introduces successful examples of single-particle oxide-coated $APbX_3$ NCs.

In 2018, our group reported $CsPbX_3/SiO_2$ [24] Janus NCs by combining a water-triggered transformation and a sol–gel strategy (Fig. 2a). Cs_4PbX_6 NCs were synthesized by a hot-injection method, then water was added to the mixture of Cs_4PbX_6 NCs and tetramethoxysilane (TMOS) under vigorous stirring. In this process, hydrophobic capping ligands (OA and OLA) on the surface of Cs_4PbBr_6 NCs are removed when CsBr is stripped out from the hexane/water interface. As a result, one side of the NCs contacting water has larger surface energy, so that SiO_2 can nucleate and grow on that side of $CsPbX_3$ NCs (Fig. 2b). This method has good universality and can be applied in the preparation of a variety of stable Janus structures. As shown in Fig. 2c, $CsPbX_3@SiO_2$ Janus structures with different halide composites were successfully prepared, which exhibit high brightness and stability. By using different oxide precursors, we successfully prepared different oxide-coated $CsPbX_3$ Janus structures, including $CsPbBr_3/ZrO_2$ [25] (Fig. 2d) and $CsPbBr_3/Ta_2O_5$ (Fig. 2e), by introducing $Zr(OC_4H_9)_4$ and tantalum(v) ethoxide as the precursor, respectively. With the protection of the oxide shell, the obtained Janus nanoparticles exhibit enhanced stability against water and light (Fig. 2f and g). Due to the small size and colloidal stability of the single-particle coating, for the first time, the coated nanoparticles were spin-coated to form a uniform film that also exhibits high stability. This work confirms the feasibility of coating $CsPbX_3$ on a single-particle scale by effectively removing the ligands on the surface of $CsPbX_3$ NCs and provides a new direction for subsequent research.

The successful preparation of Janus structures heralds the improved stability of $CsPbX_3$ NCs, which however requires further improvement due to incomplete protection. We shifted our attention to fully coated $CsPbX_3$ NCs at a single-particle level. As an amorphous material, SiO_2 has strong plasticity and is easier to fully coat onto most types of nanoparticles.[15] However, SiO_2 is a hydrophilic material that has a large contact angle (θ) with $CsPbX_3$ NCs, which are hydrophobic. Our group reported a facile one-pot approach to synthesize $CsPbBr_3/SiO_2$ core/shell NCs.[26] The formation process is shown in Fig. 3a. The precursor solution (CsBr, $PbBr_2$, OA, OLA, and ammonia dissolved in *N*,*N*-dimethylformamide) is quickly added into ultradry toluene solution containing TMOS, leading to the precipitation of product. At the very beginning of the reaction, the surface energy of NCs is high, and TMOS rapidly hydrolyzes in the presence of water and nucleates on the surface of $CsPbBr_3$ NCs. It is found that the formation rates, determined by reaction temperature, precursor species, pH value, *etc.*, are critical for the successful preparation of core/shell NCs. Monodisperse, fully coated core/shell $CsPbBr_3/SiO_2$ NCs can be realized, in which each nanoparticle has only one $CsPbBr_3$ NC (Fig. 3b). Benefitting from the full protection of the SiO_2 shell, the as-prepared core/shell structure can maintain good stability under very harsh ultrasonication treatment in aqueous solution (Fig. 3c). The full coating allows $CsPbBr_3$ NCs to be stably dispersed in aqueous solutions, which indicates potential in biological applications such as fluorescence imaging *in vivo*. The disadvantage of this method is that precise control of reaction conditions is required.

In addition to these examples, scientists have devoted many efforts to the preparation of core/shell structured perovskite NCs with different components. Tang *et al.*[27] reported $CsPbMnX_3/SiO_2$ (X = Br, Cl) core/shell NCs with two emission peaks synthesized *via* a facile reverse microemulsion method at room temperature, which can be fabricated into a stable white LED. $CsPbX_3/Al_2O_3$ structures with tunable thickness were synthesized through a general colloidal atomic layer deposition (c-ALD) method.[50] Considering that the hydrophobic ligands on $CsPbX_3$ have poor affinity with hydrophilic oxides, 3-aminopropyl triethoxysilane (APTES) was introduced as a bridging ligand to modify the surface of $CsPbX_3$, so the binding force between the oxides and $CsPbX_3$ is enhanced. After that, $CsPbX_3$/oxide (SiO_2, ZrO_2, Ta_2O_5) core/shell[28] structures were prepared, as shown in Fig. 3d. All of the core/shell NCs exhibit high stability against water, UV-light irradiation

Table 1 Summary of the structures, optical properties and stabilities of single-particle-level coated lead halide perovskite NCs

Shell materials	Compound	Structure	PL peak [nm]	PLQY (%)	Stability before coating	Stability after coating	Ref.
Oxides	$CsPbBr_3/SiO_2$	Janus	517	80	Remnant PL 17.8% after 7 days water treatment; remnant PL 84% after 6 hours light irradiation; storing in ambient for 1 days	Remnant PL 80% after 7 days water treatment; remnant PL 98% after 6 hours light irradiation; storing in ambient for 4 days	24
	$CsPbBr_3/ZrO_2$	Janus	514	90	Remnant PL 5% after 8 days water treatment; remnant PL 70% after 3 hours light irradiation	Remnant PL 80% after 8 days water treatment; remnant PL 90% after 3 hours light irradiation	25
	$CsPbBr_3/SiO_2$	Core/shell	501	90	Remnant PL 0% after storing in water for 16 min under ultrasonic treatment; storing in ambient <3 days	Remnant PL 112% after storing in water for 40 min under ultrasonic treatment; storing in ambient for 28 days	26
	$CsPbMnX_3/SiO_2$	Core/shell	446/607	54.7	Remnant PL 0% after storing in water for 6 days; remnant PL 50% after heating at 100 °C for 1 hour	Remnant PL 90% after storing in water for 6 days; remnant PL 90% after heating at 100 °C for 1 hour	27
	$CsPbI_3/SiO_2$ $CsPbI_3/ZrO_2$ $CsPbI_3/TaO_5$	Core/shell	696	51.1 57.7 59.7	Remnant PL 52–64% after 2 hours water treatment; remnant PL 67.2% after heating at 100 °C; remnant PL 25.8% after 3 hours light irradiation	Remnant PL 95–108% after 2 hours water treatment; remnant PL 85–90% after heating at 100 °C; remnant PL 52.7–62.1% after 3 hours light irradiation	28
	$CsPbBr_3/TiO_2$	Core/shell	~515	—	Remnant PL 0% after 15 min water treatment; remnant PL 37% after 24 hours light irradiation	Remnant PL 85% after 84 days water treatment; remnant PL 75% after 24 hours light irradiation	29
Semiconductors	$CsPbBr_3/Ag_2S$	Core/island	520	82	Remnant PL 0% after 4 days water treatment	Remnant PL 6.35% after 30 days water treatment	30
	$CsPbBr_3/ZnS$	Core/shell	510	—	Remnant PL 0% after 2 hours light irradiation	Remnant PL 60% after 48 hours light irradiation	31
	$CsPbBr_3/Rb_4PbBr_6$	Core/shell	507	85	Remnant PL 0% after 2 hours light irradiation	Remnant PL 90% after 42 hours light irradiation	32
	$CsPbBr_3/CdS$	Core/shell	510	90	Remnant PL 65% after 14 hours light irradiation; remnant PL ~0% after heating at 60 °C for 9 hours	Remnant PL 80% after 14 hours light irradiation; remnant PL 40% after heating at 60 °C for 9 hours	33
Metal	$CsPbBr_3$/Pt single atoms	Core/island	510	0.1	Aggregation after 20 min light irradiation by xenon lamp	Maintain structure after 60 min light irradiation by xenon lamp	34
Others	$CsPbBr_3/PbSO_4$	Core/shell	510	92	Remnant PL 44% after 150 min ethanol treatment; remnant PL 50% after 90 min acetone treatment; remnant PL 80% after 300 min light irradiation	Remnant PL 75% after 150 min ethanol treatment; remnant PL 90% after 90 min acetone treatment; remnant PL 105% after 300 min light irradiation	35
	$CsPbBr_3/ZnSO_4$	Core/shell	515	95	Anion-exchange after 40 min	No anion-exchange after 48 h	36
	$APbX_3$@PAA-*b*-PS (A = FA or Cs)	Core/shell	460–650	30–61	Quenching with added water; remnant PL 18% after 60 min light irradiation	Remnant PL 100% after storing in water for 23 days; remnant PL 92% after 60 min light irradiation	37

and thermal treatment (Fig. 3e), indicating the effective protection from the oxide shells. Surface engineering is considered an effective strategy to achieve single-particle-level full coating.

Dual-shelled $MAPbBr_3$ NCs coated by polymer and SiO_2 were also successfully prepared.[49] As shown in Fig. 3f, star-like copolymers, as nanoreactors, were designed to render the growth of core/shell NCs with controlled yet tunable perovskite core diameter, SiO_2 shell thickness and surface chemistry. The colloidal stability, chemical composition stability, photostability, and water stability of $MAPbBr_3$ NCs are dramatically improved with the protection of dual shells. This strategy can realize controllable single-particle-level coating through a smart but complex design, and we look forward to the development of a simpler and easier method.

3.2 $APbX_3$/semiconductor

As inert materials, oxides are widely used as shell materials. One disadvantage of oxides is that most of them are insulators, limiting the charge transfer between particles. In contrast, stable semiconductor materials with good carrier transport performance are good candidates. Zheng and coworkers[29] reported $CsPbBr_3/TiO_2$ core/shell NCs by calcination at 300 °C for 5 h, which allow for efficient photoinduced charge transfer and enhanced photoelectric activity during water treatment.

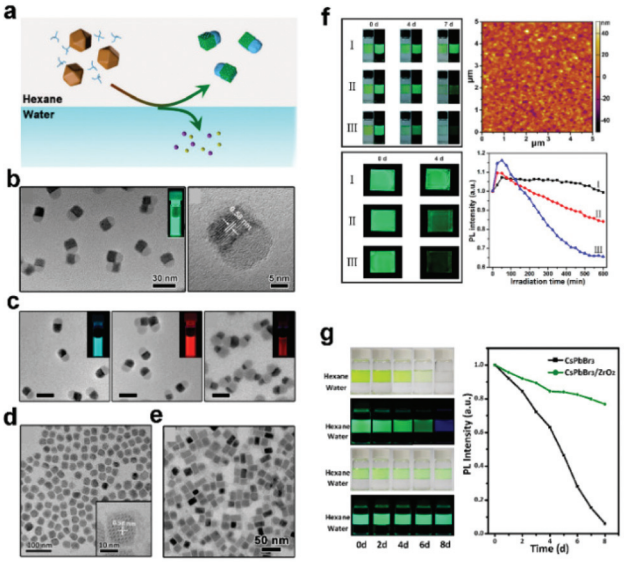

Fig. 2 (a) Schematic illustration of the formation of $CsPbX_3$/oxide Janus NCs. TEM images of (b) $CsPbBr_3/SiO_2$, (c) $CsPbX_3/SiO_2$ (X = Cl/Br or Br/I), (d) $CsPbBr_3/ZrO_2$, and (e) $CsPbBr_3/Ta_2O_5$ Janus NCs. Inset shows the corresponding photographs of the colloidal solutions. (f) High stability of $CsPbBr_3/SiO_2$ Janus NCs. Photographs show the stability against water and storage in humid air (40 °C and humidity of 75%) of (I) Janus $CsPbBr_3/SiO_2$ and $CsPbBr_3$ obtained from (II) water-triggered and (III) hot-injection methods. Atomic force microscope (AFM) image of $CsPbBr_3/SiO_2$ NC thin film. Photostability of different thin films under irradiation of 375 nm UV light. Reproduced with permission from ref. 24. Copyright 2018 American Chemistry Society. (g) High stability of Janus $CsPbBr_3/ZrO_2$ NCs. Photographs show the stability against water and the corresponding change of PL intensity. Reproduced with permission from ref. 25. Copyright 2019 American Chemistry Society.

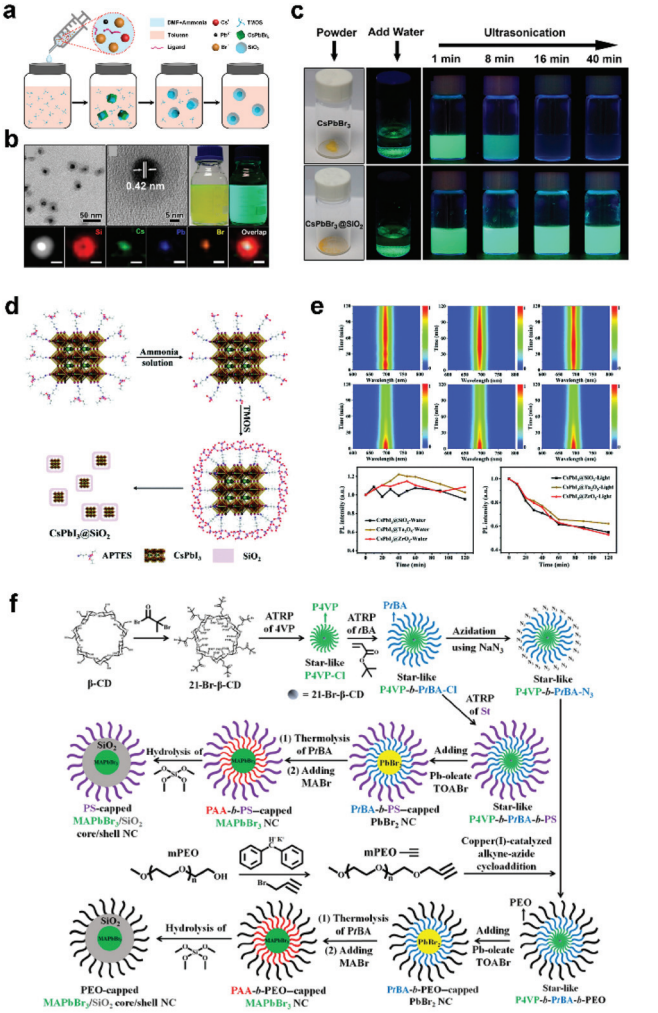

Fig. 3 (a) Formation process of $CsPbBr_3/SiO_2$ core/shell NCs. (b) TEM and EDS mapping images of $CsPbBr_3/SiO_2$ core/shell NCs. (c) High stability of $CsPbBr_3/SiO_2$ core/shell NCs against water treatment. Reproduced with permission from ref. 26. Copyright 2018 American Chemistry Society. (d) Synthetic strategy for $CsPbI_3/SiO_2$ core/shell NCs using APTES as a linking ligand. (e) High stability of $CsPbI_3/SiO_2$ core/shell NCs against water treatment. Reproduced with permission from ref. 28. Copyright 2021 Royal Society of Chemistry. (f) Stepwise representation of the synthetic route to PS-capped $MAPbBr_3/SiO_2$ core/shell NCs and PEO-capped $MAPbBr_3/SiO_2$ core/shell NCs by exploiting the star-like P4VP-*b*-PtBA-*b*-PS and P4VP-*b*-PtBA-*b*-PEO as nanoreactors, respectively. CD, cyclodextrin; BMP, 2-bromo-2-methylpropionate; and TOABr, tetraoctylammonium bromide. Reproduced with permission from ref. 49. Copyright 2019 Creative.

The decoration of $CsPbX_3$ NCs with semiconductors has attracted widespread interest to improve the stability and modify the photoelectric properties.

In addition to conventional semiconductor materials, chalcogenide quantum dots (QDs) have been widely introduced to modify $APbX_3$ NCs to regulate their photophysical properties. When semiconductors with different band gaps are compounded, different types of heterostructures can be constructed for different occasions. When applied to perovskites, the biggest challenge here is that the preparation of QDs usually requires high-temperature conditions (often higher than 250 °C) that are not friendly to perovskite NCs. For example, $CsPb(Br/I)_3$/ZnS heterostructure[53] with enhanced stability and tunable photoluminescence was prepared by a solution-phase method, in which ZnS QDs are decorated on the surface of $CsPb(Br/I)_3$ NCs. $CsPbX_3$/PbS heterostructures[51] were synthesized *via in situ* growth of PbS using hexamethyldisilathiane as the sulfur precursor. As shown in Fig. 4a and b, $CsPbX_3$/PbS NCs show tunable dual emission feature with the visible and near-infrared (NIR) PL corresponding to $CsPbX_3$ and PbS, respectively. The fluorescence of the complex can be tuned by varying the size of PbS QDs, which is realized by adjusting the reaction time (Fig. 4c and d). $CsPbBr_3$/PbS is a typical type I heterojunction. As shown in Fig. 4e and f, these tiny PbS NCs provide channels for the exciton nonradiative recombination, which can quench the PL. Moreover, results prove that exciton energy effectively transfers from $CsPbBr_3$ to PbS in $CsPbBr_3$/PbS NCs when $CsPbBr_3$ is excited, which may pave the way toward highly efficient QD photovoltaic and optoelectronic devices. Similarly, $CsPbBrI_2$/PbSe[54] and $CsPbBr_3/Ag_2S$[30] heterojunctions were reported. The QDs on $CsPbX_3$ NCs make a great contribution to the improvement of stability and the tuning of optical properties.

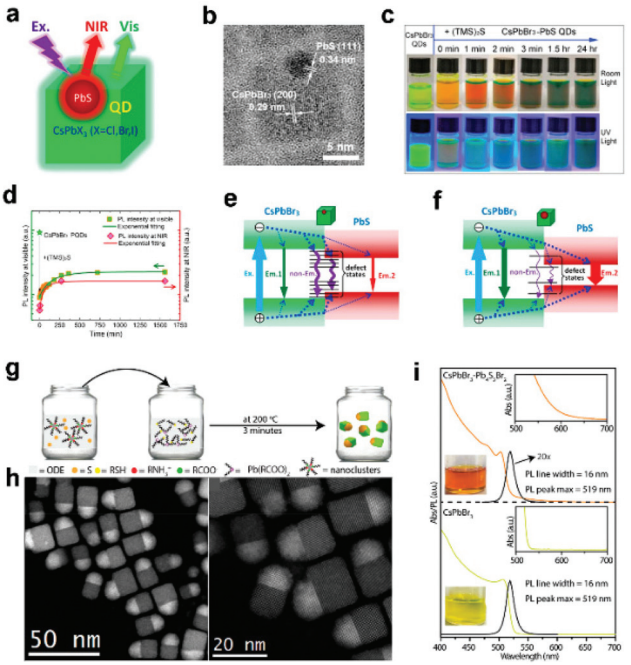

Fig. 4 (a) Schematic illustration of $CsPbX_3$/PbS heterostructure. (b) TEM image of $CsPbBr_3$/PbS heterostructure. (c) Photographs of $CsPbBr_3$ NC solution and $CsPbBr_3$/PbS NC reaction solution under daylight and UV light. (d) The intensity evolution of PL peaks in visible and NIR regions, respectively. (e, f) Scheme of the band structure and energy transfer channels of the $CsPbBr_3$/PbS NCs with increasing PbS size, respectively. Reproduced with permission from ref. 51. Copyright 2020 American Chemistry Society. (g) Scheme of the synthesis of $CsPbBr_3/Pb_4S_3Br_2$ heterostructures. (h) STEM images of $CsPbBr_3/Pb_4S_3Br_2$ NCs. (i) Absorbance and PL spectra of $CsPbBr_3/Pb_4S_3Br_2$ heterostructures and $CsPbBr_3$ NCs. Reproduced with permission from ref. 52. Copyright 2021 American Chemistry Society.

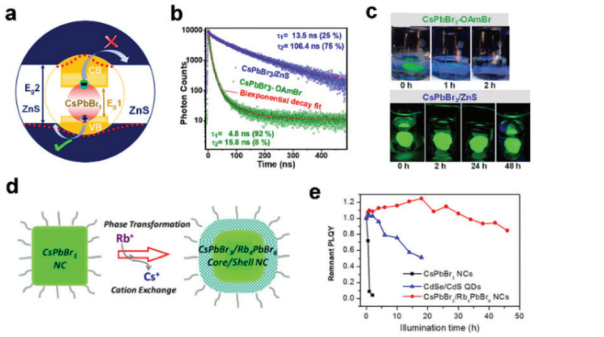

Fig. 5 (a) Schematic showing pseudo type II band alignment at the $CsPbBr_3$/ZnS core/shell interface, where the electrons are confined inside the core but the holes are delocalized over both core and shell. (b) Comparison of PL decay shows a huge increment in the PL lifetime of $CsPbBr_3$/ZnS core/shell NCs. (c) Photographs of the films of $CsPbBr_3$/ZnS core/shell NCs and $CsPbBr_3$–OLABr NCs dipped in beakers full of water and excited with UV light. Reproduced with permission from ref. 31. Copyright 2020 American Chemistry Society. (d) Schematic diagram of $CsPbBr_3/Rb_4PbBr_6$ core/shell NCs. (e) Photostability of the solution under illumination with a 450 nm LED light (175 mW cm^{-2}). Reproduced with permission from ref. 32. Copyright 2018 American Chemistry Society.

Manna's group[52] reported an interesting $CsPbX_3$ Janus heterostructure by epitaxial growth of $Pb_4S_3Br_2$ onto $CsPbBr_3$ NCs at high temperature (Fig. 4g). The sublattice of $Pb_4S_3Br_2$ is similar to that of $CsPbBr_3$, so that heterostructures can be achieved (Fig. 4h). The overall system is not just the sum of its components but a potentially valuable platform for wave function engineering strategies that are not typically accessible with halide perovskite materials due to compositional alloying. The resulting quasi type II energy level alignment at the heterojunction promotes the rapid splitting of photogenerated excitons, with the photoexcited hole localized in the chalcohalide domain and the electron partially delocalized in the entire nanostructure (Fig. 4i).

Compared to heterostructures obtained from island-like growth, core/shell heterojunctions are highly anticipated. For example, type II $CsPbBr_3$/ZnS core/shell NCs (Fig. 5a)[31] were prepared, which exhibit enhanced photoluminescence quantum yield (PLQY) and PL lifetime (Fig. 5b) and improved stability (Fig. 5c). The excellent properties of the core/shell structures lead to their various applications, such as optically pumped LEDs, photodetectors and photocatalysis. Similar $CsPbBr_3$/CdS[33,55,56] heterostructures exhibit ultrahigh chemical stability, nonblinking photoluminescence, and high quantum yield due to the reduced electronic traps within the core/shell structure. To further improve the stability, Liu and coworkers[57] synthesized a $CsPbBr_3$/nCdS/Al_2O_3 double-shell structure. The outstanding performance of $CsPbBr_3$/CdS in optoelectronic applications will be introduced in section 4.

Due to the matching of crystal lattices and similarity of elemental composition, some perovskite-like materials are employed as shell materials to achieve full encapsulation at the single-particle level. Core/shell $CsPbX_3/Cs_4PbX_6$ [58] structure was first synthesized by a hot-injection method, which opens a new way for the durability enhancement of $CsPbX_3$ NCs. In work by Tian's group,[59] amorphous $CsPbBr_x$ is introduced as the shell material to encapsulate $CsPbBr_3$ NCs, and the resulting blue-emitting $CsPbBr_3/CsPbBr_x$ nanodots display high PLQY and improved stability. Li's group[32] prepared $CsPbBr_3$ NCs enriched with lead bromide on the surface, and then added excess Rb precursor for overgrowth. As a result, $CsPbBr_3/Rb_4PbBr_6$ NCs are obtained, in which lead bromide is used as an intermediate transition layer to achieve single-particle coating (Fig. 5d). With the excellent passivation of the surface, $CsPbBr_3/Rb_4PbBr_6$ core/shell NCs show enhanced PLQY and high stability against photo treatment (Fig. 5e), enabling them to be promising in stable optoelectronic devices. $CsPbBr_3$ can also be introduced as shell material to enhance the properties of $FAPbBr_3$ NCs.[60] The disadvantage is that the instability of the ionic structure is not changed.

3.3 $CsPbX_3$/metal heterostructures

$CsPbX_3$/metal heterostructures have been carefully investigated, in which photoexcited electron–hole pairs are significantly affected by the introduction of metal. Kamat's group[63]

reported a $CsPbBr_3$/Au hybrid architecture in which Au NCs selectively grow on the corners of $CsPbBr_3$ NCs. This structure is obtained due to facilitating the reduction of $AuBr_3$ by OLA, followed by Au nucleation on the $CsPbBr_3$ surface. Moreover, Sheldon *et al.*[61,64] found that the excess $AuBr_3$ can be partially reduced to produce nonfluorescent $Cs_2Au_2Br_6$ NCs. During the process, the addition of $PbBr_2$ inhibits the substitution of Au for Pb to produce the final $CsPbBr_3$/Au heterojunction (Fig. 6a–d). The PLQY of $CsPbBr_3$ NCs is decreased when Au nanoparticles are formed on the corners of $CsPbBr_3$ NCs, suggesting the charge separation endowed by the introduction of Au. Inspired by these works, our group[62] demonstrated a reversible fluorescence switching of $CsPbI_3$ NCs by depositing and de-depositing metallic Ag nanoparticles on $CsPbI_3$ NCs controlled by light on/off, as shown in Fig. 6e–h. The controllable PL reversibility in the $CsPbX_3$/Ag composite system favors its application in smart fluorescent devices, such as a rewritable platforms. In our very recent work,[34] Pt single atoms were successfully deposited on $CsPbBr_3$ NCs through a photoassisted approach, in which the surface is partially oxidized first, followed by the anchoring of single Pt atoms through the formation of Pt–O and Pt–Br bonds. The resulting products can be used as efficient and durable catalysts for photocatalytic semi-hydrogenation of propyne. $CsPbX_3$/metal heterostructures composed of metal and semiconductor characteristics have potential prospects in the fields of optoelectronic devices and catalysis.

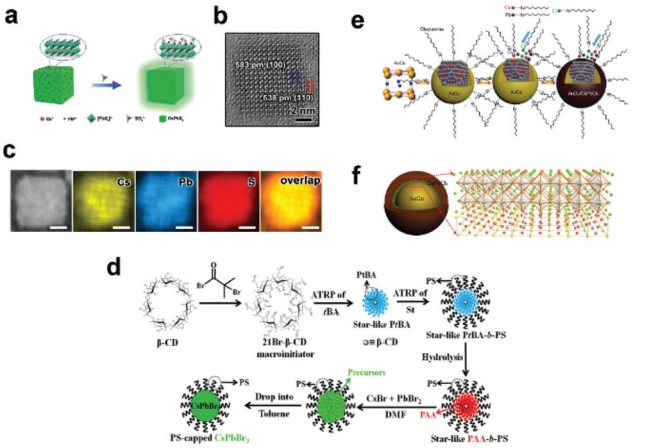

Fig. 7 (a) Schematic illustration of the post-treatment method for synthesizing $CsPbBr_3/PbSO_4$ core/shell NCs. (b) HRTEM image of one $CsPbBr_3/PbSO_4$ core/shell NC. (c) HAADF-STEM image and elemental mapping images showing the elemental distribution of Cs, Pb, and S. The scale bars are 3 nm. Reproduced with permission from ref. 35. Copyright 2021 Wiley-VCH. (d) Stepwise representation of crafting hairy all-inorganic perovskite $CsPbBr_3$ NCs intimately and permanently capped by PS chains *via* capitalizing on the amphiphilic star-like PAA-*b*-PS diblock copolymer as a nanoreactor. Reproduced with permission from ref. 65. Copyright 2019 Wiley-VCH. (e) Schematic illustration of the AuCu/$CsPbCl_3$ core/shell NCs' heteroepitaxial growth process. (f) Schematic of the AuCu/$CsPbCl_3$ core/shell NCs. Reproduced with permission from ref. 66. Copyright 2020 Wiley-VCH.

3.4 Other heterostructures

In addition to the aforementioned heterojunctions, other core/shell structures have been also studied, including $CsPbX_3$/$PbSO_4$,[35] $CsPbX_3$/polymer,[65] and AuCu/$CsPbCl_3$.[66] Our group[35] developed a post-treatment method to synthesize a $CsPbX_3$/$PbSO_4$ core/shell structure with high PLQY and stability. In this post-treatment method (Fig. 7a), octylammonium ligand is used to increase the affinity of the sulfate with the surface of $CsPbX_3$ NCs, and then the surface enriched with Pb ions is used to better react with sulfate to produce $PbSO_4$ shells (Fig. 7b and c). The presence of the $PbSO_4$ layer favors the protection of the core $CsPbX_3$ without weakening the charge transfer between $CsPbX_3$ NCs, making them suitable for stable optoelectronic devices. A general approach was demonstrated for fabricating $CsPbX_3$/metal sulfate core/shell structure.[36] The resulting core/shell NCs with a controlled shell thickness ranging from 1 to 3 nm exhibit enhanced properties in terms of colloidal stability and PLQY, providing a new opportunity for the controllable preparation of core/shell structures.

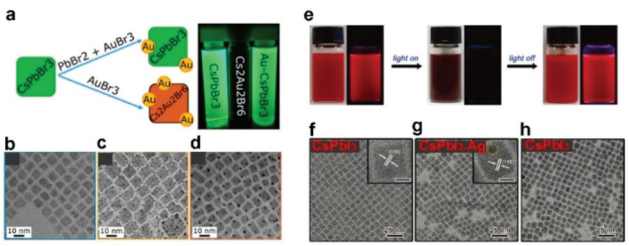

Fig. 6 (a) Schematic illustration of the formation process of $CsPbBr_3$/Au heterostructure and $Cs_2Au_2Br_6$ NCs. (b) TEM images of $CsPbBr_3$ and $CsPbBr_3$ after gold cation exchange and $CsPbBr_3$ with gold deposition. Reproduced with permission from ref. 61. Copyright 2017 American Chemistry Society. (e) Photographs showing the color change of the $CsPbI_3$/AgI composite system induced by light on/off. TEM images of (f) the original $CsPbI_3$ NCs before irradiation, (g) $CsPbI_3$/Ag NCs, and (h) $CsPbI_3$ NCs after being stored in the dark, respectively. The insets in (f) and (g) are the corresponding HRTEM images of $CsPbI_3$ and $CsPbI_3$/Ag NCs with a scale bar of 5 nm. Reproduced with permission from ref. 62. Copyright 2019 Royal Society of Chemistry.

Lin[65] reported an amphiphilic star-like block copolymer nanoreactor strategy to prepare $CsPbBr_3$/polymer NCs with high water and colloidal stabilities (Fig. 7d). The key of this method is the construction of micelles composed of amphiphilic polymers, and the precursor is well dissolved inside the micelles to form $CsPbBr_3$ NCs. The development of this strategy makes it possible for $CsPbX_3$ NCs to be used in biological imaging. $APbX_3$ (A = Cs or FA) NCs encapsulated by amphiphilic polymer (poly(acrylic acid)-*block*-poly(styrene), PAA-*b*-PS) micelles were synthesized by a room-temperature reprecipitation method.[37] The as-prepared NCs exhibit high stability against polar solvents and high-flux irradiation. The presence of polymers also prevents ion exchange between NCs, so $APbX_3$ can be directly used in white LEDs. The single-particle-level encapsulation of perovskites by organic matter is realized by the *in situ* synthesis of stable core–shell structure through

the confinement of micelles. This process is more demanding on experimental design and operation requirements.

A typical case of core/shell structure is AuCu/$CsPbCl_3$ NCs, in which AuCu NC is capped with $CsPbCl_3$ shell,[66] as shown in Fig. 7e. The same ligand OLA and hydrophobic property make it easier to overgrow $CsPbCl_3$ onto the AuCu core. Another significant reason for the core/shell structure is that the $CsPbCl_3$ shell and AuCu core maintain a high degree of lattice match (Fig. 7f).

4. Applications of core/shell structures

The encapsulation can improve the stability and photoelectric performance of bare $CsPbX_3$ NCs, making them more suitable for optoelectronic devices, which have high stability and efficiency requirements. For example, owing to the protection of SiO_2 shell and their good film-forming properties (Fig. 3f), $CsPbBr_3/SiO_2$ Janus NCs[24] have been fabricated into white LEDs (WLEDs), which can well maintain white emission after operation for one hour (Fig. 8a). In sharp contrast, the WLED made of bare $CsPbBr_3$ NCs changed from white to blue within a short period. $CsPbX_3$/semiconductor heterostructure not only improves the stability and passivates the defects of the perovskite, but also makes it more suitable for photoelectric conversion devices, such as LEDs, solar cells, photodetectors, *etc*. $CsPbI_3$/PbS core/shell NCs[67] were fabricated into electroluminescence LEDs using p–i–n structures due to $CsPbI_3$ NC films switching from n-type behavior to nearly ambipolar by PbS capping (Fig. 8b). The red LEDs exhibit dramatically enhanced operation stability, and an EQE of 11.8% can be realized. $FAPbBr_3/CsPbBr_3$ core/shell NCs[60] with high PLQY and improved stability have been utilized in a green LED, which shows excellent performance with an EQE of 8.1%. Metal–organic framework (MOF)-coated $CsPbBr_3$ NCs have been demonstrated as the emitter for bright and stable LEDs.[69] With the protection of MOFs, the as-fabricated LED shows high stability against continuous UV light irradiation, heat, and electrical stress,[69] and it is free from ion migration, NC merging, and interface corrosion. The operational lifetime of the resulting LEDs has been greatly extended. This work opens up a new way for the large-scale solution-processed fabrication of perovskite-based LEDs with high brightness and high efficiency.

$CsPbBr_3$ NCs encapsulated in a mesoporous ion-based MOF show significant interfacial charge transfer from $CsPbBr_3$ NCs to MOF, which is ideal for photocatalysis. The composite exhibits excellent and stable catalytic activities in oxygen reduction reaction (ORR) and oxygen evolution reaction (OER) when working as the synergistic photocathode in the photoassisted Li–O_2 battery. This work not only provides an efficient photoelectrocatalyst for a photoassisted Li–O_2 battery but also highlights the advantage of MOFs in stabilizing perovskites to form synergetic photocatalysts.[70] When the perovskite is combined with metals, the excited electrons and holes of the perovskite are separated, which is advantageous for catalysis. For example, our group reported the $CsPbBr_3$/Pt single atom for photocatalytic semi-hydrogenation of propyne.[34]

With the passivation of PbSe, the $CsPbI_3$/PbSe film shows a lower trap density and prolonged exciton lifetime, which promote carrier separation and collection.[68] These improvements result in high-performance $CsPbI_3$/PbSe NC solar cells with a power conversion efficiency of 13.9% and improved stability against moisture (Fig. 8c). $CsPbI_3$/PbTe NCs with enhanced structural stability were synthesized by epitaxial growth strategy. The complex was fabricated as stable WLEDs, demonstrating their potential application value in the field of indoor lighting, such as full-visible-spectrum and plant growth LEDs.[71] With the modification of $CsPbCl_3$ shell, the AuCu/$CsPbCl_3$ NCs exhibited enhanced light absorption leading to a remarkably enhanced photo-response in the nanohybrid photodetectors, which is more than 30 times that of the counterpart $CsPbCl_3$ NCs.[66] This result illustrates the feasibility of implementing the localized surface plasmon resonance light trapping directly in core/shell NCs for high-performance optoelectronics (Fig. 8d). Biocompatible $CsPbBr_3/SiO_2$ core/shell NCs[72] with no toxicity, under the protection of SiO_2, were used for bio-imaging and drug delivery. This work paves the way for new biomedical applications and processes. Highly stable $CsPbBr_3$/phTEOS-TMOS core/shell NCs have been applied to fluorescence and upconversion imaging in living cells, confirming that the perovskite NCs are suitable for various bioimaging applications.[23]

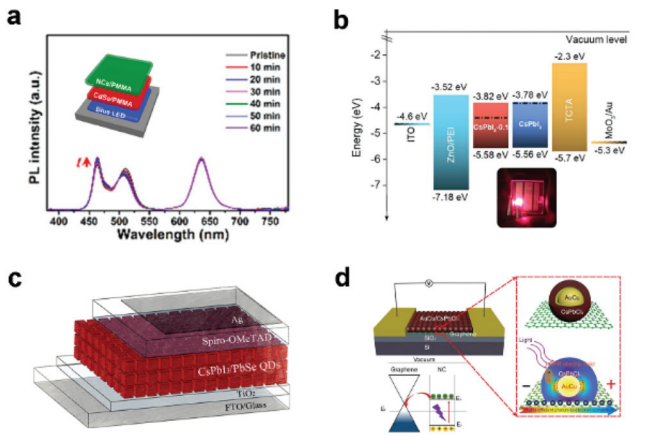

Fig. 8 (a) Time-dependent PL spectra of a WLED under continuous current of 1 mA based on $CsPbBr_3/SiO_2$ NCs. Inset shows the schematic illustration of the WLED device configuration. Reproduced with permission from ref. 24. Copyright 2018 American Chemistry Society. (b) Device energy level diagram for all functional layers in $CsPbI_3$/PbS core/shell NC-based electroluminescence LEDs. Inset shows the photograph of the working device. Reproduced with permission from ref. 67. Copyright 2018 American Chemistry Society. (c) Schematics of the device architecture of $CsPbI_3$/PbSe NC-based solar cells. Reproduced with permission from ref. 68. Copyright 2018 American Chemistry Society. (d) Schematic of the AuCu/$CsPbCl_3$ NCs nanohybrid photodetector. Reproduced with permission from ref. 66. Copyright 2020 Wiley-VCH.

5. Conclusion and outlook

In this review, we give a brief overview of the fundamental information for $APbX_3$ NCs and the reasons for their structural instability. The single-particle-level coating structures of various compositions and morphologies are summarized. Based on the excellent performance of the coated $APbX_3$ NCs, their potential applications in optoelectronic devices such as LEDs, solar cells, photodetectors, and catalysis have been introduced. However, there are still some challenges to be considered in the preparation of single-particle-level structures.

(1) At present, the shell materials and synthetic methods are monotonous. Most of the shells are oxides and chalcogenides, and the synthetic strategies focus on hot-injection and post-treatment. It is necessary to develop more shell materials and preparation approaches that can be used to improve stability and photoelectronic performance.

(2) Unlike the thickness of the shell layer grown on the surface of metal and semiconductor NCs, which can be easily controlled, it is still very difficult to tune the thickness of the shell layer on $APbX_3$ NCs. The influence of shell thickness on the photoelectric properties of $APbX_3$ NCs is worthy of attention.

(3) The coating of inert materials shows good stability against water treatment. Due to the insufficient compactness of the shell material or the existence of hydrophobic ligands, it is however impossible to obtain long-term dispersion of core/shell structures in aqueous solution, which limits their practical application.

Conflicts of interest

The authors declare no potential conflicts of interest.

Acknowledgements

This work is supported by the National Natural Science Foundation of China (51922073), Natural Science Foundation of Jiangsu Province (BK20180097), and Postdoctoral Science Foundation of China (2019M661923). We acknowledge the financial support from the 111 Project, Collaborative Innovation Center of Suzhou Nano Science, Technology (NANO-CIC) and the Priority Academic Program Development of Jiangsu Higher Education Institutions (PAPD).

Notes and references

1 H. L. Wells, *Z. Anorg. Chem.*, 1893, **3**, 195–210.
2 A. Kojima, K. Teshima, Y. Shirai and T. Miyasaka, *J. Am. Chem. Soc.*, 2009, **131**, 6050–6051.
3 L. Protesescu, S. Yakunin, M. I. Bodnarchuk, F. Krieg, R. Caputo, C. H. Hendon, R. X. Yang, A. Walsh and M. V. Kovalenko, *Nano Lett.*, 2015, **15**, 3692–3696.
4 A. Swarnkar, A. R. Marshall, E. M. Sanehira, B. D. Chernomordik, D. T. Moore, J. A. Christians, T. Chakrabarti and J. M. Luther, *Science*, 2016, **354**, 92–95.
5 M. Liu, Q. Wan, H. Wang, F. Carulli, X. Sun, W. Zheng, L. Kong, Q. Zhang, C. Zhang, Q. Zhang, S. Brovelli and L. Li, *Nat. Photonics*, 2021, **15**, 379–385.
6 J. Song, J. Li, X. Li, L. Xu, Y. Dong and H. Zeng, *Adv. Mater.*, 2015, **27**, 7162–7167.
7 Y. K. Wang, F. Yuan, Y. Dong, J. Y. Li, A. Johnston, B. Chen, M. I. Saidaminov, C. Zhou, X. Zheng, Y. Hou, K. Bertens, H. Ebe, D. Ma, Z. Deng, S. Yuan, R. Chen, L. K. Sagar, J. Liu, J. Fan, P. Li, X. Li, Y. Gao, M. K. Fung, Z. H. Lu, O. M. Bakr, L. S. Liao and E. H. Sargent, *Angew. Chem.*, 2021, **60**, 16164–16170.
8 M. Lu, Y. Zhang, S. Wang, J. Guo, W. W. Yu and A. L. Rogach, *Adv. Funct. Mater.*, 2019, **29**, 1902008.
9 L. N. Quan, B. P. Rand, R. H. Friend, S. G. Mhaisalkar, T. W. Lee and E. H. Sargent, *Chem. Rev.*, 2019, **119**, 7444–7477.
10 J. Shamsi, A. S. Urban, M. Imran, L. De Trizio and L. Manna, *Chem. Rev.*, 2019, **119**, 3296–3348.
11 A. Dey, J. Ye, A. De, E. Debroye, S. K. Ha, E. Bladt, A. S. Kshirsagar, Z. Wang, J. Yin, Y. Wang, L. N. Quan, F. Yan, M. Gao, X. Li, J. Shamsi, T. Debnath, M. Cao, M. A. Scheel, S. Kumar, J. A. Steele, M. Gerhard, L. Chouhan, K. Xu, X.-G. Wu, Y. Li, Y. Zhang, A. Dutta, C. Han, I. Vincon, A. L. Rogach, A. Nag, A. Samanta, B. A. Korgel, C.-J. Shih, D. R. Gamelin, D. H. Son, H. Zeng, H. Zhong, H. Sun, H. V. Demir, I. G. Scheblykin, I. Mora-Seró, J. K. Stolarczyk, J. Z. Zhang, J. Feldmann, J. Hofkens, J. M. Luther, J. Pérez-Prieto, L. Li, L. Manna, M. I. Bodnarchuk, M. V. Kovalenko, M. B. J. Roeffaers, N. Pradhan, O. F. Mohammed, O. M. Bakr, P. Yang, P. Müller-Buschbaum, P. V. Kamat, Q. Bao, Q. Zhang, R. Krahne, R. E. Galian, S. D. Stranks, S. Bals, V. Biju, W. A. Tisdale, Y. Yan, R. L. Z. Hoye and L. Polavarapu, *ACS Nano*, 2021, **15**, 10775–10981.
12 Q. Sun and W.-J. Yin, *J. Am. Chem. Soc.*, 2017, **139**, 14905–14908.
13 Y. Zhou and Y. Zhao, *Energy Environ. Sci.*, 2019, **12**, 1495–1511.
14 P. Reiss, M. Protiere and L. Li, *Small*, 2009, **5**, 154–168.
15 R. Ghosh Chaudhuri and S. Paria, *Chem. Rev.*, 2012, **112**, 2373–2433.
16 H. C. Wang, S. Y. Lin, A. C. Tang, B. P. Singh, H. C. Tong, C. Y. Chen, Y. C. Lee, T. L. Tsai and R. S. Liu, *Angew. Chem., Int. Ed.*, 2016, **55**, 7924–7929.
17 D. N. Dirin, L. Protesescu, D. Trummer, I. V. Kochetygov, S. Yakunin, F. Krumeich, N. P. Stadie and M. V. Kovalenko, *Nano Lett.*, 2016, **16**, 5866–5874.
18 S. Huang, Z. Li, L. Kong, N. Zhu, A. Shan and L. Li, *J. Am. Chem. Soc.*, 2016, **138**, 5749–5752.
19 M. Xing, B. Chen, J. Feng, W. Xu, Y. Bai, Y. Zhou, C. Dong, H. Zhong, J. Zhang and Y. Yin, *Chem*, 2019, **5**, 2195–2214.
20 Z. Li, L. Kong, S. Huang and L. Li, *Angew. Chem., Int. Ed.*, 2017, **56**, 8134–8138.

21 M. N. An, S. Park, R. Brescia, M. Lutfullin, L. Sinatra, O. M. Bakr, L. De Trizio and L. Manna, *ACS Energy Lett.*, 2021, **6**, 900–907.
22 L. Xu, J. Chen, J. Song, J. Li, J. Xue, Y. Dong, B. Cai, Q. Shan, B. Han and H. Zeng, *ACS Appl. Mater. Interfaces*, 2017, **9**, 26556–26564.
23 P. M. Talianov, O. O. Peltek, M. Masharin, S. Khubezhov, M. A. Baranov, A. Drabavicius, A. S. Timin, L. E. Zelenkov, A. P. Pushkarev, S. V. Makarov and M. V. Zyuzin, *J. Phys. Chem. Lett.*, 2021, **12**, 8991–8998.
24 H. Hu, L. Wu, Y. Tan, Q. Zhong, M. Chen, Y. Qiu, D. Yang, B. Sun, Q. Zhang and Y. Yin, *J. Am. Chem. Soc.*, 2018, **140**, 406–412.
25 H. Liu, Y. Tan, M. Cao, H. Hu, L. Wu, X. Yu, L. Wang, B. Sun and Q. Zhang, *ACS Nano*, 2019, **13**, 5366–5374.
26 Q. Zhong, M. Cao, H. Hu, D. Yang, M. Chen, P. Li, L. Wu and Q. Zhang, *ACS Nano*, 2018, **12**, 8579–8587.
27 X. Tang, W. Chen, Z. Liu, J. Du, Z. Yao, Y. Huang, C. Chen, Z. Yang, T. Shi, W. Hu, Z. Zang, Y. Chen and Y. Leng, *Small*, 2019, **15**, 1900484.
28 B. Tang, X. Zhao, L. J. Ruan, C. Qin, A. Shu and Y. Ma, *Nanoscale*, 2021, **13**, 10600–10607.
29 Z. J. Li, E. Hofman, J. Li, A. H. Davis, C.-H. Tung, L. Z. Wu and W. Zheng, *Adv. Funct. Mater.*, 2017, **28**, 1704288.
30 K. Fu, Y. He, B. Zhang, X. Gao and G. Zou, *J. Electroanal. Chem.*, 2020, **858**, 113835.
31 V. K. Ravi, S. Saikia, S. Yadav, V. V. Nawale and A. Nag, *ACS Energy Lett.*, 2020, **5**, 1794–1796.
32 B. Wang, C. Zhang, S. Huang, Z. Li, L. Kong, L. Jin, J. Wang, K. Wu and L. Li, *ACS Appl. Mater. Interfaces*, 2018, **10**, 23303–23310.
33 X. Tang, J. Yang, S. Li, Z. Liu, Z. Hu, J. Hao, J. Du, Y. Leng, H. Qin, X. Lin, Y. Lin, Y. Tian, M. Zhou and Q. Xiong, *Adv. Sci.*, 2019, **6**, 1900412.
34 H. Hu, W. Guan, Y. Xu, X. Wang, L. Wu, M. Chen, Q. Zhong, Y. Xu, Y. Li, T.-K. Sham, X. Zhang, L. Wang, M. Cao and Q. Zhang, *ACS Nano*, 2021, **15**, 13129–13139.
35 Q. Zhong, J. Liu, S. Chen, P. Li, J. Chen, W. Guan, Y. Qiu, Y. Xu, M. Cao and Q. Zhang, *Adv. Opt. Mater.*, 2021, **9**, 2001763.
36 F. Gao, J. Wu, Y. Zhao, T. Song, Z. Deng, P. Wang, Y. Wang and H. Li, *Nanoscale*, 2021, **13**, 10329–10334.
37 M. Imran, B. T. Mai, L. Goldoni, M. Cirignano, H. B. Jalali, F. Di Stasio, T. Pellegrino and L. Manna, *ACS Energy Lett.*, 2021, **6**, 2844–2853.
38 C. K. MØLler, *Nature*, 1958, **182**, 1436–1436.
39 J. De Roo, M. Ibanez, P. Geiregat, G. Nedelcu, W. Walravens, J. Maes, J. C. Martins, I. Van Driessche, M. V. Kovalenko and Z. Hens, *ACS Nano*, 2016, **10**, 2071–2081.
40 Q. Zhong, M. Cao, Y. Xu, P. Li, Y. Zhang, H. Hu, D. Yang, Y. Xu, L. Wang, Y. Li, X. Zhang and Q. Zhang, *Nano Lett.*, 2019, **19**, 4151–4157.
41 Y. Wei, Z. Cheng and J. Lin, *Chem. Soc. Rev.*, 2019, **48**, 310–350.
42 D. Yang, X. Li and H. Zeng, *Adv. Mater. Interfaces*, 2018, **5**, 1701662.
43 G. H. Ahmed, J. Yin, O. M. Bakr and O. F. Mohammed, *ACS Energy Lett.*, 2021, **6**, 1340–1357.
44 H. Wu, S. Lin, R. Wang, X. You and Y. Chi, *Nanoscale*, 2019, **11**, 5557–5563.
45 H. Wu, S. Wang, F. Cao, J. Zhou, Q. Wu, H. Wang, X. Li, L. Yin and X. Yang, *Chem. Mater.*, 2019, **31**, 1936–1940.
46 Y. Wei, X. Deng, Z. Xie, X. Cai, S. Liang, P. A. Ma, Z. Hou, Z. Cheng and J. Lin, *Adv. Funct. Mater.*, 2017, **27**, 1703535.
47 C. Sun, Y. Zhang, C. Ruan, C. Yin, X. Wang, Y. Wang and W. W. Yu, *Adv. Mater.*, 2016, **28**, 10088–10094.
48 Y. Duan, D. Y. Wang and R. D. Costa, *Adv. Funct. Mater.*, 2021, 2104634.
49 Y. He, Y. J. Yoon, Y. W. Harn, G. V. Biesold-McGee, S. Liang, C. H. Lin, V. V. Tsukruk, N. Thadhani, Z. Kang and Z. Lin, *Sci. Adv.*, 2019, **5**, eaax4424.
50 A. Loiudice, M. Strach, S. Saris, D. Chernyshov and R. Buonsanti, *J. Am. Chem. Soc.*, 2019, **141**, 8254–8263.
51 X. Zhang, X. Wu, X. Liu, G. Chen, Y. Wang, J. Bao, X. Xu, X. Liu, Q. Zhang, K. Yu, W. Wei, J. Liu, J. Xu, H. Jiang, P. Wang and X. Wang, *J. Am. Chem. Soc.*, 2020, **142**, 4464–4471.
52 M. Imran, L. Peng, A. Pianetti, V. Pinchetti, J. Ramade, J. Zito, F. Di Stasio, J. Buha, S. Toso, J. Song, I. Infante, S. Bals, S. Brovelli and L. Manna, *J. Am. Chem. Soc.*, 2021, **143**, 1435–1446.
53 W. Chen, J. Hao, W. Hu, Z. Zang, X. Tang, L. Fang, T. Niu and M. Zhou, *Small*, 2017, **13**, 1604085.
54 J. Zhang, X. Liu, P. Jiang, H. Chen, Y. Wang, J. Ma, R. Zhang, F. Yang, M. Wang, J. Zhang and G. Tu, *Nano Energy*, 2019, **66**, 104142.
55 X. Tang, J. Yang, S. Li, W. Chen, Z. Hu and J. Qiu, *Front. Chem.*, 2019, **7**, 499.
56 J. Shi, W. Ge, J. Zhu, M. Saruyama and T. Teranishi, *ACS Appl. Nano Mater.*, 2020, **3**, 7563–7571.
57 X. Liu, X. Zhang, L. Li, J. Xu, S. Yu, X. Gong, J. Zhang and H. Yin, *ACS Appl. Mater. Interfaces*, 2019, **11**, 40923–40931.
58 C. Jia, H. Li, X. Meng and H. Li, *Chem. Commun.*, 2018, **54**, 6300–6303.
59 S. Wang, C. Bi, J. Yuan, L. Zhang and J. Tian, *ACS Energy Lett.*, 2017, **3**, 245–251.
60 C. Zhang, S. Wang, X. Li, M. Yuan, L. Turyanska and X. Yang, *Adv. Funct. Mater.*, 2020, **30**, 1910582.
61 B. J. Roman, J. Otto, C. Galik, R. Downing and M. Sheldon, *Nano Lett.*, 2017, **17**, 5561–5566.
62 P. Li, D. Yang, Q. Zhong, Y. Zhang, M. Chen, S. Jiang, J. Chen, M. Cao, Q. Zhang and Y. Yin, *Nanoscale*, 2019, **11**, 3193–3199.
63 S. K. Balakrishnan and P. V. Kamat, *ACS Energy Lett.*, 2017, **2**, 88–93.
64 F. A. Rodriguez Ortiz, B. J. Roman, J. R. Wen, N. Mireles Villegas, D. F. Dacres and M. T. Sheldon, *Nanoscale*, 2019, **11**, 18109–18115.
65 Y. J. Yoon, Y. Chang, S. Zhang, M. Zhang, S. Pan, Y. He, C. H. Lin, S. Yu, Y. Chen, Z. Wang, Y. Ding, J. Jung, N. Thadhani, V. V. Tsukruk, Z. Kang and Z. Lin, *Adv. Mater.*, 2019, **31**, 1901602.

66 M. Gong, M. Alamri, D. Ewing, S. M. Sadeghi and J. Z. Wu, *Adv. Mater.*, 2020, **32**, 2002163.
67 X. Zhang, M. Lu, Y. Zhang, H. Wu, X. Shen, W. Zhang, W. Zheng, V. L. Colvin and W. W. Yu, *ACS Cent. Sci.*, 2018, **4**, 1352–1359.
68 S. Wang, C. Bi, A. Portniagin, J. Yuan, J. Ning, X. Xiao, X. Zhang, Y. Y. Li, S. V. Kershaw, J. Tian and A. L. Rogach, *ACS Energy Lett.*, 2020, **5**, 2401–2410.
69 H. Tsai, S. Shrestha, R. A. Vilá, W. Huang, C. Liu, C.-H. Hou, H.-H. Huang, X. Wen, M. Li, G. Wiederrecht, Y. Cui, M. Cotlet, X. Zhang, X. Ma and W. Nie, *Nat. Photonics*, 2021, **15**, 843–849.
70 G. Y. Qiao, D. Guan, S. Yuan, H. Rao, X. Chen, J. A. Wang, J. S. Qin, J. J. Xu and J. Yu, *J. Am. Chem. Soc.*, 2021, **143**, 14253–14260.
71 L. Zhang, M. Zhu, Y. Sun, J. Zhang, M. Zhang, H. Zhang, F. Zhou, J. Qu and J. Song, *Nano Energy*, 2021, **90**, 106506.
72 P. Kumar, M. Patel, C. Park, H. Han, B. Jeong, H. Kang, R. Patel, W. G. Koh and C. Park, *J. Mater. Chem. B*, 2020, **8**, 10337–10345.